Soil Dynamics and Earthquake Engineering 102 (2017) 65–74

Contents lists available at ScienceDirect

Soil Dynamics and Earthquake Engineering

journal homepage: www.elsevier.com/locate/soildyn

Empirical correlations between the effective number of cycles and other intensity measures of ground motions

Wenqi Du[a,*], Gang Wang[b]

[a] Institute of Catastrophe Risk Management, Nanyang Technological University, 50 Nanyang Avenue Singapore

[b] Dept. of Civil and Environmental Engineering, The Hong Kong University of Science and Technology, Clear Water Bay, Kowloon Hong Kong

ARTICLE INFO

Keywords:
Effective number of cycles
Correlation coefficient
NGA database
Ground motion selection
Liquefaction potential

ABSTRACT

The effective number of cycles is an important ground motion parameter for the assessment of liquefaction potential. In this paper, empirical correlations for two measures of the effective number of cycles with seven amplitude-, cumulative-, and duration-based intensity measures (IMs) are studied and compared, based on the NGA strong motion database and several ground motion prediction equations. The adopted definitions of the effective number of cycles include an absolute measure (N_A) and a relative measure (N_R). It is shown that N_A is highly correlated with high-frequency IMs, such as spectral acceleration (SA) at short periods, Arias intensity, and negatively correlated with signification durations (Ds). On the other hand, N_R shows generally negative correlations with both amplitude- and cumulative-based IMs. N_R also exhibits small-to-moderate positive correlations with Ds, which are commonly regarded as similar parameters to the effect number of cycles. Simple parametric functions are provided to describe the N_A-SA and N_R-SA correlations for various cases. The importance of considering multiple IMs rather than SA only in ground-motion selection is also briefly demonstrated.

1. Introduction

The number of cycles of ground motions has been widely recognized as one of the critical parameters in geotechnical earthquake engineering. Many studies (e.g., [1,2]) have concluded that the number of cycles of shakings is strongly correlated with the buildup of pore water pressure in liquefiable soils. As summarized by Hancock and Bommer [3], there are dozens of definitions to count the effective number of cycles, by converting all irregular amplitude cycles to an equivalent number of uniform cycles. The concept of equivalent number of cycles is commonly used for evaluating liquefaction potential [4–6].

Due to the complex features of ground motion time histories, single ground motion intensity measure (IM) cannot adequately characterize earthquake loadings. Therefore, a set of IMs (vector-IMs) is often required in some practical applications, such as the estimation of earthquake-induced slope displacement [7,8]. Since current ground motion prediction equations (GMPEs) only provide the means and standard deviations for specific IMs, empirical correlations among the residuals of these IMs are then the key requirement to contrast the joint distribution of vector-IMs. These empirical correlations are indispensable in vector-based probabilistic seismic hazard analysis [9] and scenario-based ground motion selection approaches, e.g., [10–12].

Recently a number of researchers have studied empirical correlations between the residuals of multiple IMs, such as spectral accelerations (SA) at multiple periods, Arias intensity (Ia), cumulative absolute velocity (CAV), and significant durations (Ds), e.g., [13–18]. However, to the knowledge of the authors, there are no existing correlation models involving the number of effective cycles. Bommer et al. [19] has studied the correlations between several duration parameters and effective numbers of ground motion cycles. Yet, they did not aim at evaluating the correlations between the residuals of these IMs, making it difficult to be used in some applications such as ground motion selection.

The objective of this paper is to examine the empirical correlations between the effective number of cycles and other commonly used IMs. The definitions of these employed IMs are firstly discussed, associated with the utilized GMPEs and ground motion database. Secondly, the estimated correlation coefficients between the residuals of these IMs are presented; simple parametric models are also proposed to readily predict the empirical correlations. The influence of rupture distance (R_{rup}) on the resulting correlation coefficients is then examined. Finally, based on the correlation results, some recommendations are provided regarding the use of different definitions of the effective number of cycles for practical applications.

* Corresponding author.
E-mail address: wqdu@ntu.edu.sg (W. Du).

http://dx.doi.org/10.1016/j.soildyn.2017.08.014
Received 17 November 2015; Received in revised form 9 July 2017; Accepted 25 August 2017
0267-7261/

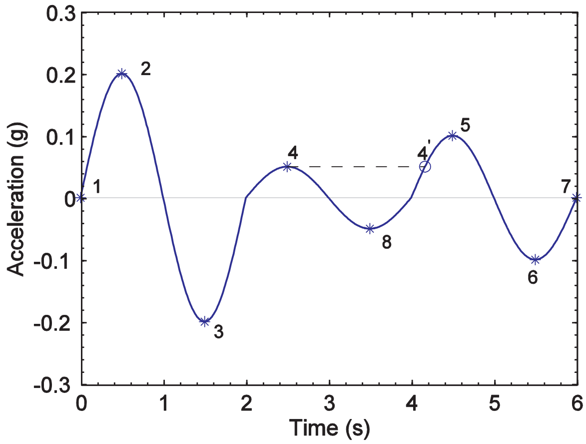

Fig. 1. A demonstrated example of the use of rainflow-counting approach. This segment consists of several sine waves, which can be counted as five half cycles (1–2; 2–3; 3-4-4′ – 5; 5–6 and 6–7) and one full cycle (4–8-4′). The amplitudes of the five half cycles are 0.1, 0.2, 0.15, 0.1, and 0.05 g, respectively; the amplitude of the full cycle is 0.05 g. The segment yields values of N_A and N_R as 0.09 and 1.125, respectively.

2. Selected IMs and ground motion database

2.1. Effective number of cycles

As summarized in Hancock and Bommer [3], there are many cycle-counting definitions in the literature, which can be mainly classified into several categories: peak counting, level crossing counting, range counting, and indirect counting methods. These cycle-counting definitions were developed for low-cycle fatigue testing [20]. Among these definitions, the rainflow range-counting method is the most popular since it quantifies both the high-frequency and low-frequency cyclic waves in broadband signals. This method counts a history of peaks and troughs in sequence which can be regarded as starting and ending points for defining each cycle. The algorithm can be simplified as: (i), the signal is turned clockwise as 90°; (ii), an imagined source of water will flow down the "pagoda roofs" from their upper tops; (iii), the water will drip down when it reaches the edge. It will stop when it comes to a point that is already wet (quantified by previous flow), or it reaches opposite beyond the vertical of the starting point; (iv), the steps (ii)-(iii) can be repeated to get a series of half-cycles. The detailed algorithm of this approach can be found in References [3,21]. Fig. 1 shows a simple example about the application of the rainflow-counting technique. Total five half-cycles and one full-cycle are identified for this wave. Besides, prediction equations for the effective number of cycles based on the rainflow-counting approach have been proposed [22], which can be directly used to account for the statistical distributions of these IMs.

Similar to the cyclic damage parameter for low-cycle fatigue failure used by Malhotra [23], the absolute definition of the effective number of cycles can be expressed as:

$$N_A = \sum_{i=1}^{2T_n} u_i^2 \tag{1}$$

where u_i is the amplitude of the i-th half cycle obtained by the rainflow range-counting method; T_n is the total number of cycles; and N_A is the absolute measure of the effective number of cycles. It is noted that the exponent coefficient is set as 2 herein, which reflects the relative importance of different amplitude cycles. A higher value of the exponent coefficient represents a larger contribution caused by large-amplitude cycles.

Relative definitions of the effective number of cycles are commonly used in earthquake engineering. A typical relative definition of the number of cycles, in which each amplitude u_i is normalized by the maximum amplitude of all half-cycles, $u_{\max}$, is expressed as:

$$N_R = \frac{1}{2}\sum_{i=1}^{2T_n}\left(\frac{u_i}{u_{\max}}\right)^2 \tag{2}$$

where N_R is the relative measure of the effective cycles. A value of 2 is also adopted for the exponent coefficient.

It is worth noting that only the effective number of cycles obtained by the rainflow-counting method is considered in this paper, due to its popularity and robustness. The selected measures of cyclic numbers can be applied in most practical cases. The aforementioned empirical equations proposed by Stafford and Bommer [22], which are termed as SB09 model hereafter, will be used to predict N_A and N_R in the following section. The SB09 model utilized a subset of the Pacific Earthquake Engineering Research (PEER) NGA-West1 database [24], employing moment magnitude M_w, rupture distance R_{rup}, site parameters and the depth to the top of rupture (Z_{tor}) as indicators. A set of equations has been proposed by Stafford and Bommer [22], while only the basic equations without the consideration of Z_{tor} or directivity effect are used in this study. The median predictions of the SB09 model for N_A and N_R with respect to M_w and R_{rup} are shown in Fig. 2. It should be noted that the other few prediction equations using different counting methods, e.g., [25], are not considered due to the scope of this paper.

2.2. Other IMs considered

The other IMs considered herein are listed as: (a) peak values of ground motion time histories, including peak ground acceleration (PGA) and peak ground velocity (PGV); (b) SA at multiple periods; (c) cumulative-based intensity measures, including Ia and CAV; and (d) ground motion duration parameters, including significant durations defined as time intervals over which 5–75% and 5–95% of Ia are built

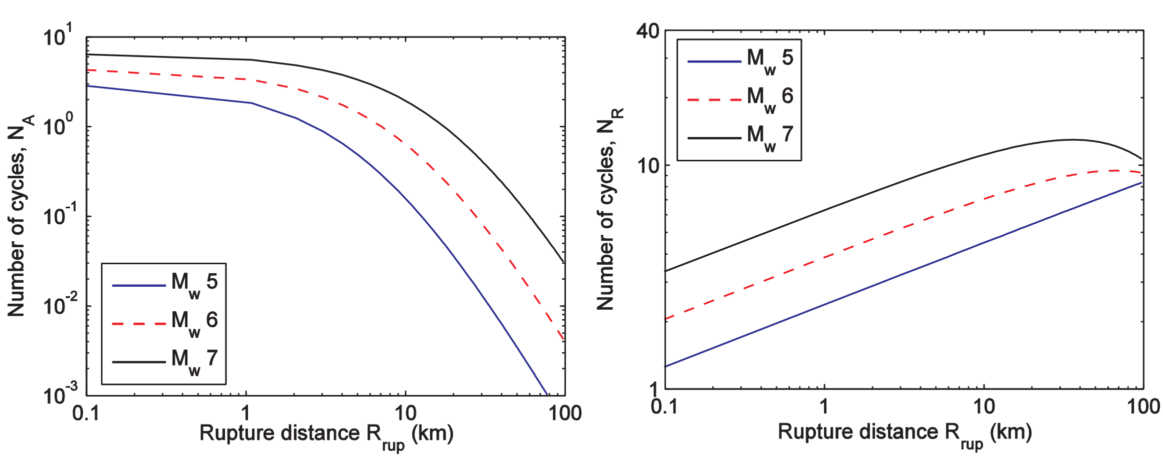

Fig. 2. Median predictions of the SB09 model for the effective number of cycles N_A and N_R, respectively. The V_{s30} value is set as 400 m/s for predicting N_R.

Table 1
Summary of the IMs considered in this study.

IM parameters	Definition*	GMPEs used	
		Abbreviations	Reference
N_A	Shown in Eq. (1)	SB09	Stafford and Bommer [22]
N_R	Shown in Eq. (2)		
PGA	$\max(\lvert a(t)\rvert)$	AS08	Abrahamson and Silva [26]
		BA08	Boore and Atkinson [27]
PGV	$\max(\lvert v(t)\rvert)$	CB08	Campbell and Bozorgnia [28]
SA(T)	Peak response of a linear elastic system	CY08	Chiou and Youngs [29]
Ia	$\frac{\pi}{2g}\int_0^{t_{\max}} a(t)^2 dt$ [44]	TBA03	Travasarou et al. [30]
		FS12	Foulser-Piggott and Stafford [31]
		CB12	Campbell and Bozorgnia [32]
CAV	$\int_0^{t_{\max}} \lvert a(t)\rvert\ dt$ [45]	CB10	Campbell and Bozorgnia [33]
		DW13	Du and Wang [34]
$Ds_{5\text{-}75}$	Time interval between 5% to 75% of Ia	KS06	Kempton and Stewart [35]
$Ds_{5\text{-}95}$	Time interval between 5% to 95% of Ia	BSA09	Bommer et al. [36]
		DW17	Du and Wang [37]

* a(t): Acceleration-time history; v(t):velocity-time history; t_{max}: total duration of the ground motion time history and g is gravitational acceleration.

up (termed as $Ds_{5–75}$ and $Ds_{5–95}$, respectively). The selected IMs cover a range of amplitude-, intensity-, and duration-based parameters, representing various characteristics of earthquake loadings. The IMs considered as well as their definitions are summarized in Table 1.

Several GMPEs are needed to predict the statistical distributions (medians and standard deviations) of these IMs. For PGA, PGV, and SA, since the SB09 model for N_A and N_R was developed using the NGA-West1 database, it seems not necessary to select the recently proposed NGA-West2 GMPEs. Instead, the GMPEs of the NGA-West1 project for shallow crustal earthquakes in active tectonic regions are adopted: Abrahamson and Silva [26], Boore and Atkinson [27], Campbell and Bozorgnia [28], and Chiou and Youngs [29]. They are referred to as AS08, BA08, CB08, and CY08, respectively. The GMPEs proposed by Travasarou and Bray [30], Foulser-Piggott and Stafford [31], and Campbell and Bozorgnia [32] are chosen to estimate the statistical distribution of Ia. For CAV, only two GMPEs [33,34] were developed using the global ground motion database, so they are adopted.

The GMPEs proposed by Kempton and Stewart [35] (KS06), Bommer et al. [36] (BSA09), and Du and Wang [37] (DW17) are used for predicting the significant durations $Ds_{5–75}$ and $Ds_{5–95}$. The KS06 model was developed based on the analysis of magnitude effects on source duration, while the BSA09 and DW17 models were empirically derived using subsets of the NGA database. Only the base function (without the consideration of fault type or directivity effect) of the KS06 model is used herein. All the selected GMPEs as well as their abbreviations are also summarized in Table 1.

2.3. Ground motion database

A subset of the NGA database is selected to calculate the empirical values of the IMs considered. The ground motion database selected is almost identical to that used in deriving the CB08 model [28], including 1560 recordings from 64 earthquakes with moment magnitudes from 4.3 to 7.9 and rupture distances from 0.1 to 199 km. The complete recording list regarding the database can be found in Campbell and Bozorgnia [38]. Fig. 3(a) shows the distribution of moment magnitude and rupture distance contained in the database.

It should be noted that each recorded time history has a usable period range, in order to eliminate low-frequency or high-frequency noises. Therefore, SA at periods larger than the maximum usable period should not be used for subsequent correlation analyses. The number of usable ground motions is expected to decrease as vibration period increases, as is shown in Fig. 3(b).

3. Empirical correlation analyses

3.1. Computational procedures for correlation coefficients

Current GMPEs usually assume that IMs are logarithmically normally distributed, which can be shown as:

$$\ln(IM_i) = \overline{\ln(IM_i)} + \eta_i + \varepsilon_i \tag{3}$$

where $\ln(IM_i)$ and $\overline{\ln(IM_i)}$ denote the measured (geometric mean of two horizontal components of each record) and the predicted logarithmic i-th IM (e.g., SA, Ia, N_A), respectively. η_i and ε_i represent the inter-event and intra-event residuals of the i-th IM (normally distributed with zeros means and standard deviations τ and σ), respectively. The total standard deviation σ_T is given as $\sigma_T^2 = \sqrt{\tau^2 + \sigma^2}$. The values of τ, σ, and σ_T for various IMs are generally provided by GMPEs.

The Pearson product-moment correlation coefficient is a widely used measure of linear correlation between two variables [39]. The correlation coefficients between the inter-event or intra-event residuals of different IMs can be estimated as:

$$\rho_{x_1,x_2} = \frac{\sum_{i=1}^{n}(x_1^{(i)} - \bar{x}_1)(x_2^{(i)} - \bar{x}_2)}{\sqrt{\sum_{i=1}^{n}(x_1^{(i)} - \bar{x}_1)^2 \sum_{j=1}^{n}(x_2^{(j)} - \bar{x}_2)^2}} \tag{4}$$

where x_1 and x_2 are random variables (e.g., η_1 and η_2 for the inter-event residuals of IM_1 and IM_2); n is the total number of the random variables considered (i.e., number of earthquakes for the inter-event correlation, or number of ground motion records for the intra-event correlation); and $\bar{x}_1$ and $\bar{x}_2$ denote the sample mean of variables x_1 and x_2, respectively. In this paper, IM_1 refers to N_A or N_R, and IM_2 refers to the other aforementioned measures such as PGA, SA, and Ia. For each pair of IMs, ρ_{η_1,η_2} and $\rho_{\varepsilon_1,\varepsilon_2}$ can be computed via Eq. (4).

Under the assumption that η_i and ε_i are independent [40], the correlation between the total residuals can be expressed as:

$$\rho_{\varepsilon_{T1},\varepsilon_{T2}} = \frac{1}{\sigma_{T_1}\cdot\sigma_{T_2}}\left(\rho_{\eta_1,\eta_2}\tau_1\tau_2 + \rho_{\varepsilon_1,\varepsilon_2}\sigma_1\sigma_2\right) \tag{5}$$

where τ_k, σ_k, and σ_{Tk} (k = 1, 2) are the standard deviations of the inter-event, intra-event, and total residuals for the k-th IM, respectively. Thus, the correlation between the total residuals for each pair of IMs can be calculated via Eqs. (4) and (5) accordingly.

The above statistical analysis only provides the point-estimate of the correlation coefficient, while the uncertainty of ρ should also be accounted for carefully. Such uncertainty is due to the finite number of sample size, as well as different ground motion models used in its determination. A bootstrap method is often used to construct the confidence intervals of correlation coefficients [39]. The basic idea of this method is to re-sample the observed dataset by random sampling with replacement from the original dataset, and then the correlation coefficients of these bootstrap replicates can be calculated. This process needs to be repeated a certain number of times to accurately estimate the variance of ρ.

In addition to the bootstrap method, another widely used method is the Fisher z transformation [41]. This method converts the correlation coefficient ρ into a transformed variable z via:

$$z = \frac{1}{2}\ln\left(\frac{1+\rho}{1-\rho}\right) = \tanh^{-1}\rho \tag{6}$$

where ρ is the Pearson correlation coefficient; $\tanh^{-1}$ is the inverse

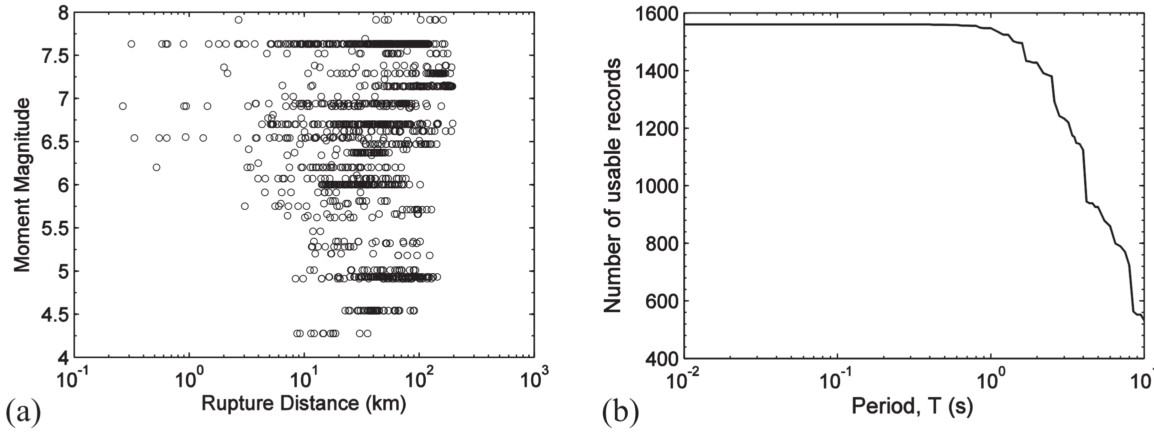

Fig. 3. (a) Distribution of earthquake recordings with respect to moment magnitude and rupture distance used in this study; (b) the number of usable records to compute the correlation of N_A and N_R with SA at different periods.

hyperbolic tangent function; and z is the transformed correlation coefficient which is approximately normally distributed. The variance of ρ usually becomes smaller when it approaches 1 or −1, whereas the variance of the transformed variable z can keep approximately constant for all ρ values. Therefore, if the mean and standard deviation of the transformed variable z are denoted as μ_z and σ_z, respectively, the corresponding median correlation coefficient ρ_{50} can be computed as:

$$\rho_{50} = \left(\frac{e^{2\mu_z} - 1}{e^{2\mu_z} + 1}\right) = \tanh(\mu_z) \tag{7}$$

Similarly, a certain percentile of ρ can be obtained using μ_z and σ_z (e.g., $\rho_{84} = \tanh(\mu_z + \sigma_z)$; $\rho_{16} = \tanh(\mu_z - \sigma_z)$).

3.2. Correlations of cyclic numbers with PGA, PGV, and SA

Fig. 4 shows the distributions of the computed correlation coefficients of N_A, N_R with PGA and PGV, respectively. For each pair of the IMs, the correlation coefficient ρ between the total residuals was first estimated via Eqs. (4) and (5); 1500 bootstrap replicates from the original dataset were then generated for quantifying the uncertainty of ρ. Boxplots are used to show the uncertainty caused by the finite sample size (obtained by the bootstrap method); the results obtained by the

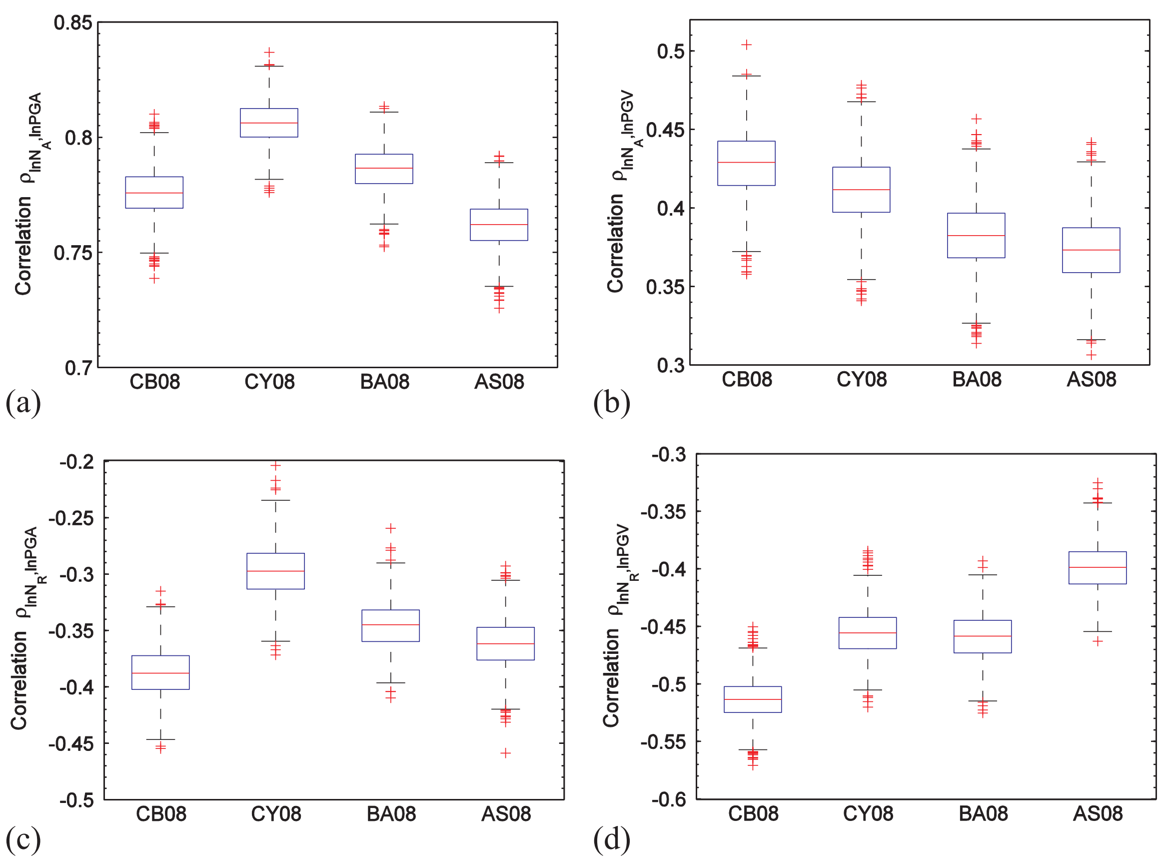

Fig. 4. Computed correlation coefficients between (a) N_A and PGA, (b) N_A and PGV, (c) N_R and PGA, (d) N_R and PGV. In these and subsequent boxplots, the central red line denotes the median of the data (50th percentile), and the edges of the box (blue lines) mark the 25th and 75th percentiles. The ends of the whiskers represent the 0.35th and 99.65th percentiles, respectively; the red plus symbols denote outliers. The results obtained by various GMPEs are shown in each subplot. (For interpretation of the references to color in this figure legend, the reader is referred to the web version of this article.)

four aforementioned GMPEs are shown in each boxplot. Fig. 4(a) and (b) illustrate that the correlations of N_A with PGA and PGV are positive with median values of approximately 0.78 and 0.4, respectively. This is not surprising, since N_A represents the summation of the amplitude for each half cycle, which is expected to be larger if PGA of a ground motion is higher. Fig. 4(c) and (d) show the computed correlations of N_R with PGA and PGV, respectively. Unlike the case of N_A, the correlations of N_R-PGA and N_R-PGV are generally negative, with median values of approximately −0.36 and −0.46, respectively. Hence, as a relative definition, N_R has a much weaker correlation with PGA compared with N_A because of the normalization process. For PGV, N_R exhibits slightly stronger correlation than N_A, although the N_R-PGV correlation is found to be negative. Besides, it can also be seen that the uncertainty (i.e., 25th and 75th percentiles represented by the edges of the box) due to the finite sample size is generally in the range of 0.02–0.03, whereas the variability from the use of different GMPEs is more notable. There appears to be no specific GMPE which yields systematically higher or lower correlations. The results (a number of ρ based on the bootstrap method) obtained by various GMPEs were combined together in a logic-tree framework with equal weight assigned. The combined results were then transformed via Eq. (6) to evaluate μ_z and σ_z. The calculated median correlation coefficients ρ_{50}, as well as σ_z are listed in Table 2.

Fig. 5 shows the computed empirical correlations [Eq. (5)] between N_A, N_R and SA versus vibration period. Similar to the results shown in Fig. 4, the correlations of N_A-SA are generally positive, while the N_R-SA correlations are negative. As seen in Fig. 5(a), the correlation of N_A-SA is generally constant for $T < 0.2\ s$, and it shows a decreasing trend as period T increases for $T > 0.2\ s$. This implies that N_A is mainly dependent on the high-frequency content of ground motions. On the other hand, the correlation of N_R-SA is in the range of −0.4 to −0.1. It generally increases with increasing vibration period for $T < 0.1\ s$ and $T > 1\ s$, whereas a noticeable decreasing trend of ρ can be observed for periods from 0.1 s to 1 s. The variation of the N_R-SA correlation versus period is presently not feasible to explain. Yet, the overall small correlation indicates that N_R can represent additional ground motion characteristics compared to SA.

Based on the aforementioned bootstrap and z transformation approaches, the computed median, 16th and 84th percentiles (blue dashed lines) of the correlation coefficients for N_A-SA and N_R-SA are illustrated in Fig. 6(a) and (b), respectively. A smooth parametric function is usually desirable for practical use. The following piecewise linear function is then proposed to fit the median N_A-SA and N_R-SA correlations:

$$\rho_{\mathrm{Nx,SA}} = a_n + \frac{\ln(T/T_n)}{\ln(T_{n+1}/T_n)}(a_{n+1} - a_n) \quad T_n \le T \le T_{n+1} \tag{8}$$

where N_x denotes N_A or N_R in this paper; a_n and T_n are regressed parameters in order to capture the overall shape of the correlation coefficients over the whole period range. The values of these parameters are listed in Table 3. For any give T, ρ can be predicted by linear interpolation in logarithmic period scale. The solid lines in Fig. 6 are obtained by the proposed parametric function [Eq. (8)], and they compare reasonably well with the empirical data. Besides, it can also be observed that the variations of ρ for the N_A-SA and N_R-SA correlations versus period T are relatively small. The computed values of σ_z are in the ranges of 0.03–0.07 and 0.03–0.05 for N_A-SA and N_R-SA correlations, respectively. Therefore, it seems not necessary to accurately capture the small variations of σ_z with periods, and the σ_z values of 0.05 and 0.04 can be directly used for N_A-SA and N_R-SA over the whole period range. The predicted 16th and 84th percentiles using the constant σ_z values are also shown (black dotted line) in Fig. 6.

Table 2
Computed median correlation coefficients ρ_{50} and standard deviations σ_z of the transformed variable z for N_A and N_R with PGA, PGV, Ia, CAV, Ds_{5-75}, and Ds_{5-95}, respectively. σ_z is given in parentheses.

	PGA	PGV	Ia	CAV	Ds_{5-75}	Ds_{5-95}	N_R
N_A	0.78 (0.057)	0.40 (0.043)	0.79 (0.13)	0.64 (0.061)	−0.27 (0.045)	−0.29 (0.035)	0.03 (0.025)
N_R	−0.35 (0.046)	−0.46 (0.057)	−0.19 (0.032)	−0.04 (0.029)	0.51 (0.056)	0.37 (0.064)	–

3.3. Correlation of cyclic numbers with Ia and CAV

Fig. 7(a) and (b) display the computed correlations (e.g., the median, 25th, and 75th percentiles) of N_A with Ia and CAV, respectively. It is not surprising that the N_A-Ia and N_A-CAV correlations are moderately positive, given that both Ia and CAV, as measures of the cumulative intensity of shakings, are highly dependent on the absolute amplitudes of ground motion cycles. The correlation between N_A and Ia is slightly larger than that of N_A-CAV. This is possibly due to the fact that both N_A and Ia employ 2 as the exponent coefficient in their definitions. Besides, noticeable differences among the correlations by various GMPEs can be observed for both figures. Such uncertainty could be quantified using the aforementioned bootstrap and z transformation methods.

Fig. 7(c) and (d) display the computed correlations of N_R with Ia and CAV, respectively. As observed previously, there are slight variations in the correlations obtained by using different GMPEs. The median correlation coefficients of N_R with Ia and CAV are approximately −0.19 and −0.04, respectively. The rather poor correlations imply that, the cumulative-based IMs (Ia, CAV) are relatively independent of the relative definition of the effective cyclic number (N_R). It should be noted that the median correlation coefficients ρ_{50}, and the standard deviations σ_z between N_A, N_R, PGA, PGV, Ia, CAV, and subsequent Ds_{5-75} and Ds_{5-95}, are summarized in Table 2.

3.4. Correlation of cyclic numbers with $Ds_{5\text{-}75}$ and $Ds_{5\text{-}95}$

Fig. 8(a) and (b) show the calculated correlation coefficients of N_A with Ds_{5-75} and Ds_{5-95}, respectively. It can be seen that the N_A-Ds_{5-75} and N_A-Ds_{5-95} correlations are generally similar, with median values in the range of −0.35 to −0.2, respectively. The negative correlations imply that a ground motion with a longer than expected Ds would possibly have a smaller than expected N_A value. Fig. 8(c) and (d) illustrate the calculated correlation coefficients of N_R with Ds_{5-75} and Ds_{5-95}, respectively. Both the N_R-Ds_{5-75} and N_R-Ds_{5-95} correlations are some degree of positive, while the correlation between N_R and Ds_{5-75} is slightly larger.

The observed correlations between N_A, N_R and Ds_{5-75}, Ds_{5-95} are consistent with physical intuitions. As discussed previously, N_A is highly correlated with PGA, and it has been studied that Ds_{5-75} and Ds_{5-95} are negatively correlated with peak amplitudes (PGA, PGV) of ground motions [14]. Therefore, it is not surprising that the N_A-Ds_{5-75} and N_A-Ds_{5-95} correlations are negative. On the other hand, the normalized measure N_R shows some degree of positive correlations with significant durations. Since Ds_{5-75} and Ds_{5-95} represent the time interval across which a great amount of seismic energy is dissipated, a ground motion with longer Ds_{5-75} or Ds_{5-95} is likely to be more numbers of cyclic waves (and hence larger N_R). Besides, Bommer et al. [19] also studied the correlations between ground motion durations and the effective cyclic numbers. They computed the correlations directly based on the measured values of the IMs, without the consideration of GMPEs and residuals of these IMs. Therefore, the results presented in this study are different with those provided in Reference [19].

Fig. 9(a) and (b) show the distribution of the inter-event and intra-event residuals between N_A and N_R, respectively. The data points of these two figures are almost randomly distributed, with the computed correlation coefficients as +0.15 and −0.04, respectively. The correlation coefficient between the total residuals using Eq. (5) is calculated

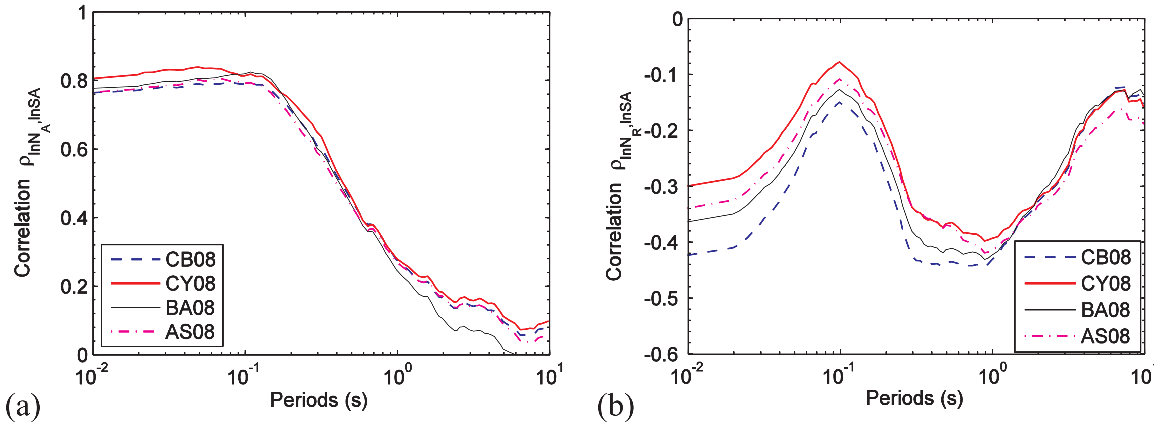

Fig. 5. Computed correlation coefficients [Eq. (5)] for (a) N_A and SA; (b) N_R and SA, respectively.

as 0.03. Such poor correlation indicates that, although both N_A and N_R represent the effective numbers of cycles of a ground motion, the physical interpretations of these two measures are significantly different. Therefore, N_A and N_R are better suited for different applications.

4. Influence of rupture distance on N_A-SA and N_R-SA correlations

It is tempting to examine the influence of causal parameters (i.e., M_w, R_{rup}) on the N_A-SA and N_R-SA correlations. The influence of magnitude M_w on the correlations is found to be less significant than R_{rup}. Therefore, only the influence of rupture distance on the correlations is investigated in this section.

The empirical residuals are divided into three distance bins, namely R_{rup} = 0–30 km, 30–80 km, and 80–200 km, respectively. The number of usable records in each distance bin versus spectral period is shown in Fig. 10, from which it can be seen that each distance bin includes an adequate number of data points in order to yield statistically stable results. The procedures introduced in Section 3.1 were used for the correlation calculations based on the binned empirical data. Fig. 11 demonstrates the resulting N_A-SA and N_R-SA correlations for the three distance bins. For the N_A-SA correlations, it can be seen that the far-distance (R_{rup} = 80–200 km) records exhibit the strongest correlations over a wide period range; the correlations for moderate-distance (R_{rup} = 30–80 km) records are noticeably larger than those of short-distance records (R_{rup} = 0–30 km) at periods larger than 2 *s*. For the N_R-SA correlations, the moderate-distance ground motions exhibit the strongest correlations for T < 1 *s*, while the far-distance ground motions yield the strongest correlations for T > 1 *s*. Such differences can be attributed to the different ground motion characteristics caused by travelling distances. It has been widely studied that long travelling distance tends to filter out high-frequency components of seismic waves, resulting in (far-distance) ground motions consisting of mainly moderate-to-long period seismic waves.

Table 3
Coefficients for predicting the N_A-SA and N_R-SA correlations.

n	N_A-SA (T)		N_R-SA (T)	
	a_n	T_n	a_n	T_n
1	0.79	0.01	−0.37	0.01
2	0.80	0.15	−0.32	0.03
3	0.25	1.0	−0.12	0.10
4	0.15	2.0	−0.43	0.5
5	0.02	10.0	−0.35	2.0
6	–	–	−0.15	5.0
7	–	–	−0.15	10.0

For practical usage, piecewise linear functions [Eq. (8)] are also developed to fit the correlation data for each distance bin. The regressed a_n and T_n parameters for the distance-binned N_A-SA and N_R-SA correlations are summarized in Tables 4, 5, respectively. As illustrated in Fig. 11, the proposed piecewise linear curves approximate the empirical data reasonably well. Besides, as listed in Tables 4, 5, a constant σ_z value is also assigned for each distance bin to quantify the uncertainty of N_A-SA and N_R-SA correlations. Compared to the σ_z values obtained based on the whole ground motion database, the distance-binned σ_z values are slightly larger, due to the decrease of the available number of data points in each distance bin.

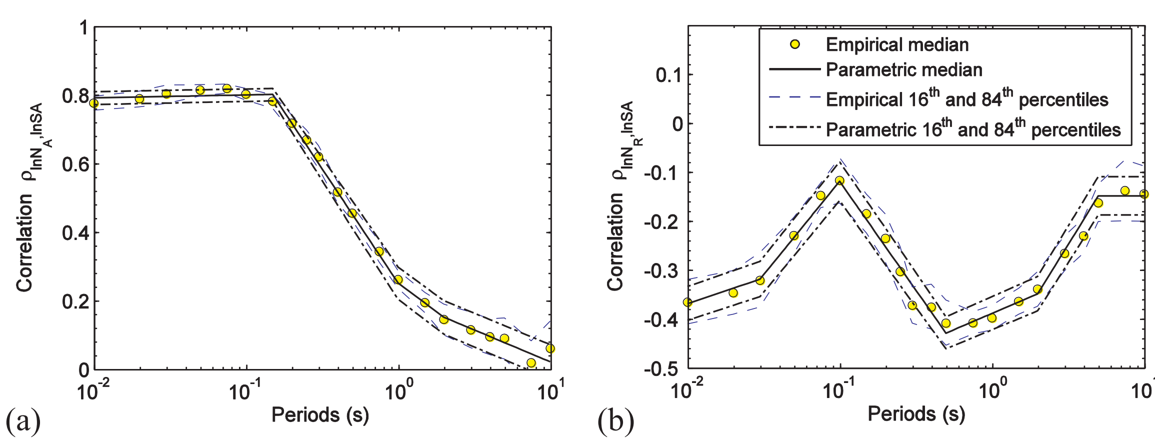

Fig. 6. Comparisons of the empirical correlations and the piece-wise linear fitting curves for (a) N_A and SA, (b) N_R and SA, respectively.

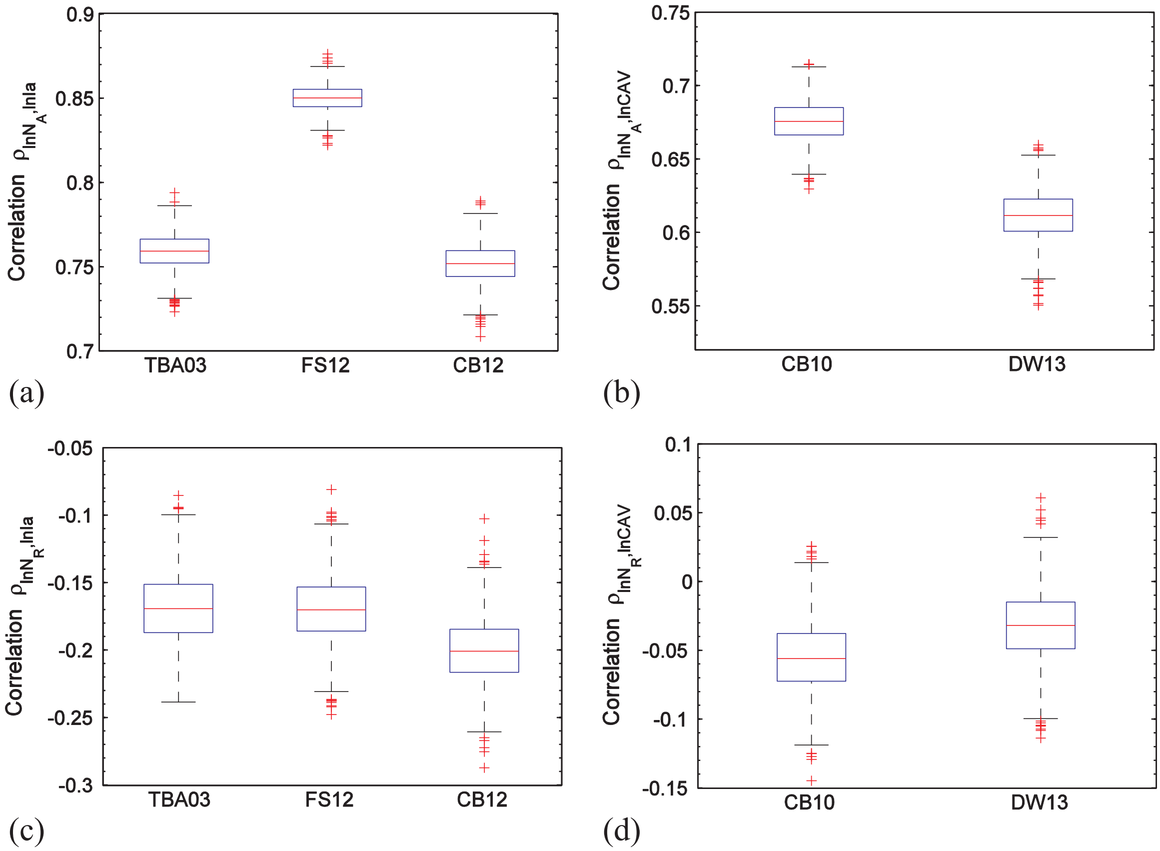

Fig. 7. Correlation coefficients between (a) N_A and Ia, (b) N_A and CAV, (c) N_R and Ia, (d) N_R and CAV. The results obtained by various GMPEs are shown in each subplot.

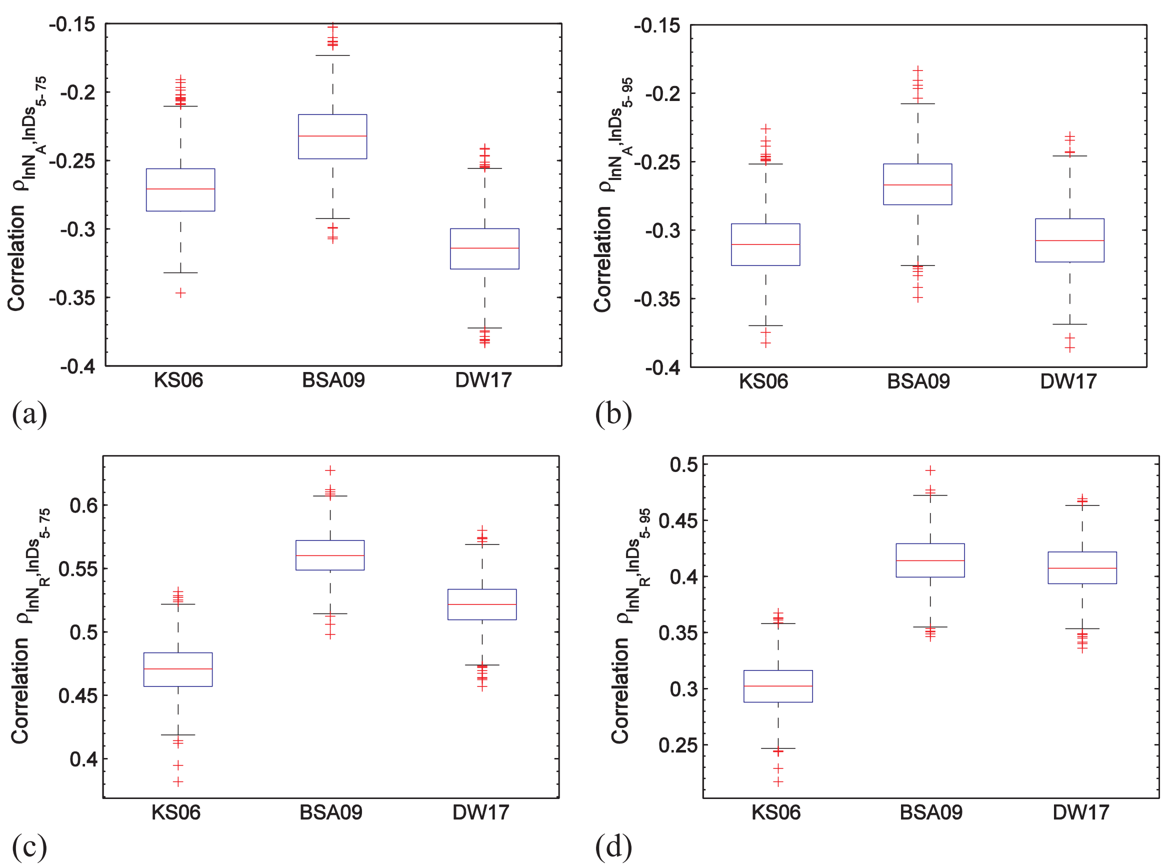

Fig. 8. Correlation coefficients between (a) N_A and $Ds_{5–75}$, (b) N_A and $Ds_{5–95}$, (c) N_R and $Ds_{5–75}$, (d) N_R and $Ds_{5–95}$. The results obtained by various GMPEs are shown in each subplot.

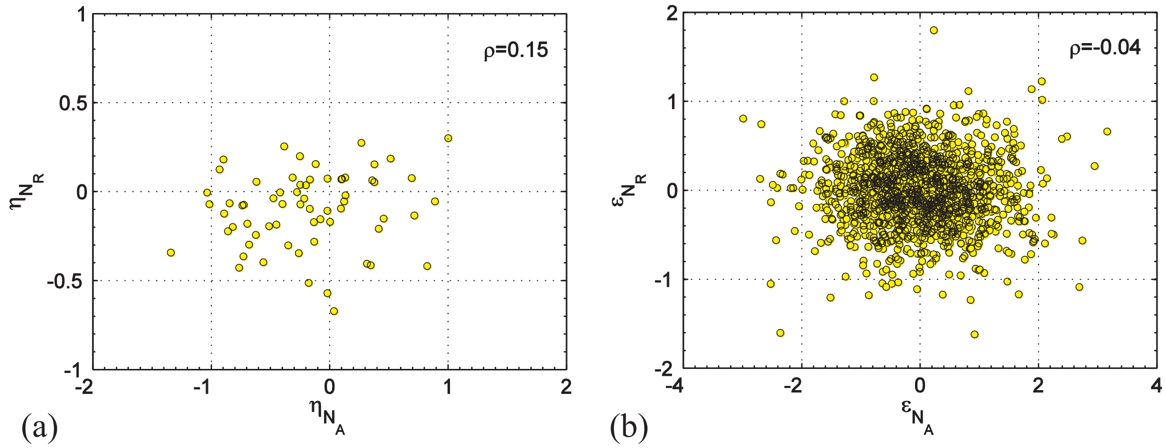

Fig. 9. Distributions of (a) inter-event and (b) intra-event residuals between N_A and N_R.

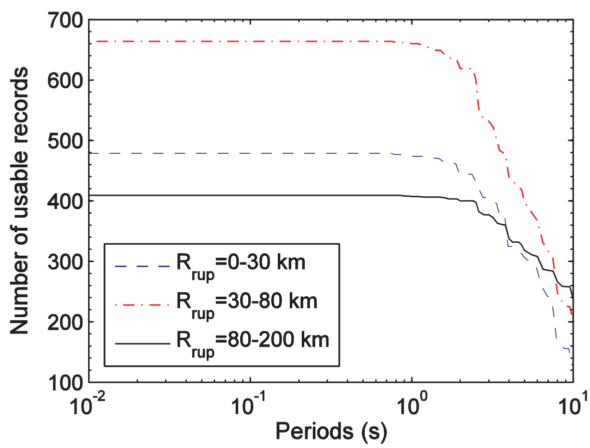

Fig. 10. Number of usable records versus spectral periods in each distance bin.

Table 4
N_A-SA correlations for different rupture distance bins.

Distances (km)	0–30		30–80		80–200	
n	a_n	T_n	a_n	T_n	a_n	T_n
1	0.75	0.01	0.79	0.01	0.82	0.01
2	0.79	0.1	0.83	0.12	0.83	0.15
3	0.65	0.25	0.66	0.25	0.48	0.75
4	0.25	1.0	0.24	0.75	0.19	2.0
5	0.04	4.0	0.11	2.0	0.22	4.0
6	−0.06	10	0.11	10.0	0.03	10.0
σ_z	0.07		0.06		0.07	

Table 5
N_R-SA correlations for different rupture distance bins.

Distances (km)	0–30		30–80		80–200	
n	a_n	T_n	a_n	T_n	a_n	T_n
1	−0.38	0.01	−0.44	0.01	−0.34	0.01
2	−0.13	0.05	−0.36	0.03	−0.30	0.03
3	−0.09	0.13	−0.12	0.1	−0.11	0.1
4	−0.36	0.4	−0.47	0.35	−0.33	0.3
5	−0.37	1.0	−0.42	1.5	−0.44	1.2
6	−0.25	3.0	−0.09	6.0	−0.19	7.0
7	0.0	10.0	−0.15	10.0	−0.28	10.0
σ_z	0.07		0.06		0.07	

5. Discussions

The effective number of cycles is an important measure in geotechnical earthquake engineering, especially in the evaluation of liquefaction potential. The number of ground motion cycles may also influence the degree of seismic damage on structures. Therefore, it would be desirable if the effective number of cycles could be used for a variety of applications. Of the two measures of effective number of cycles considered in this study, N_A is the absolute definition (calculated based on the absolute amplitude of cycles), while N_R is the relative definition in which all cycles are normalized by the maximum

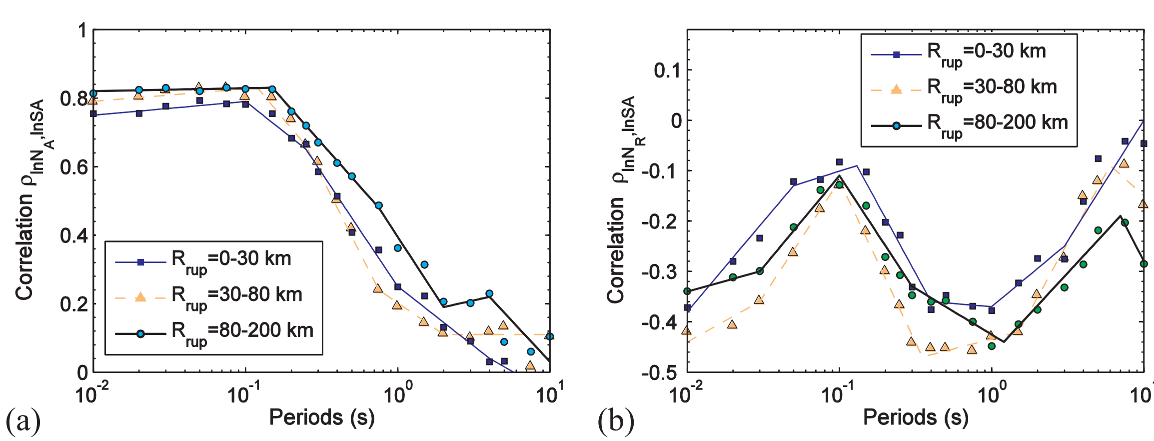

Fig. 11. (a) N_A-SA correlations and (b) N_R-SA correlations for different rupture distance bins (empirical data and fitting functions are represented as symbols and lines, respectively).

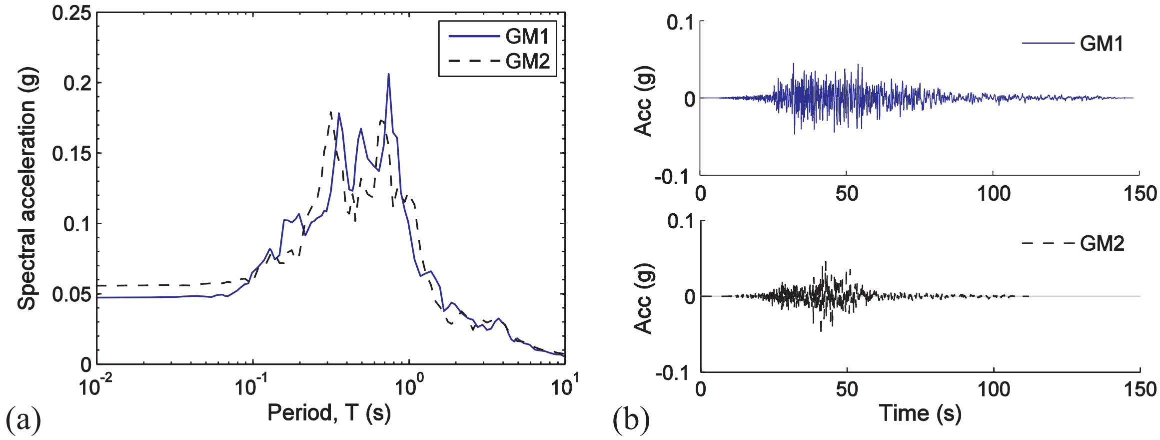

Fig. 12. Comparisons of (a) response spectra, (b) time histories of a pair of spectrally equivalent ground motions. GM1 is recorded at the CHY023 station during the 1999 Chi-Chi earthquake; GM2 is also from the Chi-Chi earthquake recorded at the TAP098 station, scaled by a factor of 1.02.

amplitude of cycles. It has been found that N_A is highly correlated with high-frequency IMs such as PGA, Ia, and SA at short periods. Compared to PGA, N_A considers not only the effect of the single cycle with peak amplitude, but also the effect of a number of secondary cycles. Hence, N_A can be regarded as a surrogate of PGA in some cases, in which the estimation of cyclic deformation demand is important [42]. In contrast, N_R exhibits small-to-moderate negative correlations with PGA, PGV, Ia, and SA, indicating that N_R can provide some supplementary information regarding the ground motion characteristics compared with these IMs. Therefore, although N_R alone may not be very useful, N_R in conjunction with primary IMs (e.g., PGA, SA) would be favorable in some engineering applications.

It is not surprising that N_A, as an amplitude-based indicator, exhibits negative correlations with Ds_{5-75} and Ds_{5-95}. The correlations of N_R with Ds_{5-75} and Ds_{5-95} are just moderately positive (with maximum ρ_{50} as 0.51), which may contradict the assumption that duration measures can effectively represent the number of cycles of ground motions. These results are some degree of consistent with a previous study which stated that the correlations between ground motion durations and the number of effective cycles are weak [19].

For demonstration purpose, Fig. 12 shows the comparisons of response spectra and time histories for a pair of ground motions. A spectrally equivalent method, which minimizes the sum of the squared errors between two response spectra, is used to select the two ground motions. It can be seen that although the two response spectra are generally comparable, the numbers of the effective cycles of time histories are significantly different. The computed N_R and Ds_{5-75} values for GM1 are 18.8 and 26 s, while the corresponding N_R and Ds_{5-75} for GM2 are 8.5 and 19.8 s, respectively. In such a case, N_R is apparently a better indicator than Ds_{5-75} to differentiate the two ground motions, and therefore, N_R should be incorporated in the ground motion selection process for some engineering applications.

It is worth noting that, both the two measures (N_A and N_R) studied in this paper are defined using an exponent coefficient of 2. Yet, some studies (e.g., [43]) have reported that the effective number of cycles defined with an exponent coefficient of 3 is more appropriate for evaluating the liquefaction potential of clean sands. Thus, the correlation results presented in this paper should be used with caution for the liquefaction analysis of such soil materials. Due to the lack of robust predictive models, the correlation study related to the measures of effective cyclic number defined as an exponent coefficient of 3 is currently not feasible. It will be a subject of future study.

6. Conclusions

This manuscript studied the empirical correlations between the effective number of ground motion cycles and other commonly used intensity measures (IMs), including PGA, PGV, spectral accelerations (SA), Ia, CAV, Ds_{5-75}, and Ds_{5-95}. The NGA strong motion database and several globally applicable GMPEs have been utilized for calculating the correlation coefficients between these IMs. Two definitions of the effective number of cycles, namely N_A (absolute measure) and N_R (relative measure) are considered in this paper. It was found that N_A has strong positive correlations ($\rho \approx 0.8$) with high-frequency IMs such as PGA, Ia, and SA at $T < 0.2$ *s*; moderate positive correlations with PGV, CAV, and SA over a period range of 0.2–1 *s*; and weak negative correlations ($\rho \approx -0.3$) with significant durations. The observed correlation results can be explained by the fact that N_A is mainly determined by larger-amplitude ground motion cycles, and it can be classified as a high-frequency amplitude-based IM.

The relative measure N_R generally exhibits small-to-moderate negative correlations with amplitude-based (e.g., PGA, PGV) and cumulative intensity-based IMs (Ia, CAV). This means that N_R can provide additional information regarding the ground motion characteristics compared with these amplitude- and cumulative-based IMs. Besides, it was observed that N_R is moderately correlated ($\rho < 0.6$) with significant duration parameters, indicating that the duration parameters cannot perfectly represent the effective number of ground motion cycles.

The influence of rupture distance on the N_A-SA and N_R-SA correlations was also examined. It was found that the far-distance ground motions tend to exhibit stronger N_A-SA and N_R-SA correlations, especially at long spectral periods. A set of piecewise linear functions were proposed to quantify the N_A-SA and N_R-SA correlations for general and various distance-binned cases. The derived correlation coefficients and the parametric equations can be easily used in vector-based seismic hazard analysis or ground motion selection for scenario earthquakes. A simple example was provided to demonstrate that ground motions selected based on SA only may result in a biased representation of other IMs. Specifically, the correlation results described herein could be used to select a suite of well-representative ground motions, to assess earthquake-induced risks such as liquefaction potential.

Acknowledgments

The work described in this paper was supported by Hong Kong Research Grants Council through Collaborative Research Fund grant No. PolyU8/CRF/13G and General Research Fund grant No. 16213615. The authors thank two anonymous reviewers for their helpful comments to improve this manuscript.

References

[1] Seed HB, Lee KL. Liquefaction of saturated sands during cyclic loading. J Soil Mech Found Div 1966;92(6):105–34.
[2] Martin GR, Finn WL, Seed HB. Fundementals of liquefaction under cyclic loading. J Geotech Geoenviron Eng (ASCE) 1975. [101(ASCE# 11231 Proceeding)].
[3] Hancock J, Bommer JJ. The effective number of cycles of earthquake ground motion. Earthq Eng Struct Dyn 2005;34(6):637–64.
[4] Annaki M, Lee KL. Equivalent uniform cycle concept for soil dynamics. J Geotech Eng Div (ASCE) 1977;103(6):549–64.
[5] Kramer SL. Geotechnical earthquake engineering. New Jersey: Practice Hall; 1996. p. 653.
[6] Green RA, Terri GA. Number of equivalent cycles concept for liquefaction evaluations—Revisited. J Geotech Geoenviron Eng 2005;131(4):477–88.
[7] Rathje EM, Saygili G. Probabilistic seismic hazard analysis for the sliding displacement of slopes: scalar and vector approaches. J Geotech Geoenviron Eng 2008;134(6):804–14.
[8] Du W, Wang G. Fully probabilistic seismic displacement analysis of spatially distributed slopes using spatially correlated vector intensity measures. Earthq Eng Struct Dyn 2014;43(5):661–79.
[9] Baker JW, Cornell AC. A vector-valued ground motion intensity measure consisting of spectral acceleration and epsilon. Earthq Eng Struct Dyn 2005;34(10):1193–217.
[10] Wang G. A ground motion selection and modification method capturing response spectrum characteristics and variability of scenario earthquakes. Soil Dyn Earthq Eng 2011;31(4):611–25.
[11] Jayaram N, Lin T, Baker JW. A computationally efficient ground-motion selection algorithm for matching a target response spectrum mean and variance. Earthq Spectra 2011;27(3):797–815.
[12] Bradley BA. A ground motion selection algorithm based on the generalized conditional intensity measure approach. Soil Dyn Earthq Eng 2012;40:48–61.
[13] Baker JW, Jayaram N. Correlation of spectral acceleration values from NGA ground motion models. Earthq Spectra 2008;24(1):299–317.
[14] Bradley BA. Correlation of significant duration with amplitude and cumulative intensity measures and its use in ground motion selection. J Earthq Eng 2011;15(6):809–32.
[15] Bradley BA. Empirical correlations between peak ground velocity and spectrum-based intensity measures. Earthq Spectra 2012;28(1):17–35.
[16] Bradley BA. Correlation of arias intensity with amplitude, duration and cumulative intensity measures. Soil Dyn Earthq Eng 2015;78:89–98.
[17] Wang G, Du W. Empirical correlations between cumulative absolute velocity and spectral accelerations from NGA ground motion database. Soil Dyn Earthq Eng 2012;43:229–36.
[18] Du W. Empirical correlations of frequency content parameters of ground motions with other intensity measures. J Earthq Eng 2017. http://dx.doi.org/10.1080/13632469.2017.1342303. (published online).
[19] Bommer JJ, Hancock J, Alarcón JE. Correlations between duration and number of effective cycles of earthquake ground motion. Soil Dyn Earthq Eng 2006;26(1):1–13.
[20] Dowling NE. Fatigue failure predictions for complicated stress-strain histories. J Mater 1972;7(1):71–87.
[21] Amzallag C, Gerey JP, Robert JL, Bahuaud J. Standardization of the rainflow counting method for fatigue analysis. Int J Fatigue 1994;16(4):287–93.
[22] Stafford PJ, Bommer JJ. Empirical equations for the prediction of the equivalent number of cycles of earthquake ground motion. Soil Dyn Earthq Eng 2009;29(11):1425–36.
[23] Malhotra PK. Cyclic-demand spectrum. Earthq Eng Struct Dyn 2002;31(7):1441–57.
[24] Chiou B, Darragh R, Gregor N, Silva W. NGA project strong-motion database. Earthq Spectra 2008;24(1):23–44.
[25] Liu AH, Stewart JP, Abrahamson NA, Moriwaki Y. Equivalent number of uniform stress cycles for soil liquefaction analysis. J Geotech Geoenviron Eng 2001;127(12):1017–26.
[26] Abrahamson NA, Silva WJ. Summary of the Abrahamson & Silva NGA ground-motion relations. Earthq Spectra 2008;24(1):67–97.
[27] Boore DM, Atkinson GM. Ground-motion prediction equations for the average horizontal component of PGA, PGV and 5%-damped PSA at spectral periods between 0.01s and 10 s. Earthq Spectra 2008;24(1):99–138.
[28] Campbell KW, Bozorgnia Y. NGA ground motion model for the geometric mean horizontal component of PGA, PGV, PGD and 5% damped linear elastic response spectra for periods ranging from 0.1 to 10 s. Earthq Spectra 2008;24(1):139–71.
[29] Chiou BJ, Youngs RR. An NGA model for the average horizontal component of peak ground motion and response spectra. Earthq Spectra 2008;24(1):173–215.
[30] Travasarou T, Bray JD. Empirical attenuation relationship for Arias Intensity. Earthq Eng Struct Dyn 2003;32(7):1133–55.
[31] Foulser-Piggott RF, Stafford PJ. A predictive model for Arias intensity at multiple sites and consideration of spatial correlations. Earthq Eng Struct Dyn 2012;41(3):431–51.
[32] Campbell KW, Bozorgnia Y. A comparison of ground motion prediction equations for Arias intensity and cumulative absolute velocity developed using a consistent database and functional form. Earthq Spectra 2012;28(3):931–41.
[33] Campbell KW, Bozorgnia Y. A ground motion prediction equation for the horizontal component of cumulative absolute velocity (CAV) based on the PEER-NGA strong motion database. Earthq Spectra 2010;26(3):635–50.
[34] Du W, Wang G. A simple ground-motion prediction model for cumulative absolute velocity and model validation. Earthq Eng Struct Dyn 2013;42(8):1189–202.
[35] Kempton JJ, Stewart JP. Prediction equations for significant duration of earthquake ground motions considering site and near-source effects. Earthq Spectra 2006;22(4):985–1013.
[36] Bommer JJ, Stafford PJ, Alarcón JE. Empirical equations for the prediction of the significant, bracketed, and uniform duration of earthquake ground motion. Bull Seismol Soc Am 2009;99(6):3217–33.
[37] Du W, Wang G. Prediction equations for ground-motion significant durations using the NGA-West2 database. Bull Seismol Soc Am 2017;107(1):319–33.
[38] Campbell KW, Bozorgnia Y. Campbell-Bozorgnia NGA ground motion relations for the geometric mean horizontal component of peak and spectral ground motion parameters. Berkeley: Pacific Earthquake Engineering Research Center, University of California; 2007. p. 238. (PEER Report No. 2007/02).
[39] Ang AHS, Tang WH. Probability concepts in engineering: emphasis on applications in civil and environmental engineering. John Wiley & Sons; 2007.
[40] Abrahamson NA, Youngs RR. A stable algorithm for regression analysis using the random effects model. Bull Seismol Soc Am 1992;82(1):505–10.
[41] Kutner MH, Nachtsheim CJ, Neter J. Applied linear regression models. 4th edition McGraw-Hill; 2004.
[42] Kunnath SK, Chai YH. Cumulative damage-based inelastic cyclic demand spectrum. Earthq Eng Struct Dyn 2004;33(4):499–520.
[43] Idriss IM, Boulanger RW. Soil liquefaction during earthquakes. Earthquake Engineering Research Institute; 2008. (MNO-12).
[44] Arias A. A measure of earthquake intensity. In: Hansen RJ, editor. Seismic design for nuclear power plants. Cambridge, MA: MIT Press; 1970. p. 438–83.
[45] Electrical Power Research Institute (EPRI). A criterion for determining exceedance of the operating basis earthquake, Report No. EPRI NP-5930, Palo Alto, California; 1988.